

# Supporting Information

## **Bimetal alloy anchored on biomass-derived porous N-doped carbon fibers as self-supporting bifunctional oxygen electrocatalysts for flexible Zn-air batteries**

Yanli Niu, Xue Teng, Shuaiqi Gong and Zuofeng Chen\*

*School of Chemical Science and Engineering, Tongji University, Shanghai 200092,  
China*

---

\*Corresponding author

E-mail address: zfchen@tongji.edu.cn (Z. F. Chen)

## **Experimental section**

### **Materials**

Nickel(II) chloride hexahydrate ( $\text{NiCl}_2 \cdot 6\text{H}_2\text{O}$ ,  $\geq 99.9\%$ ), ferrous chloride tetrahydrate ( $\text{FeCl}_2 \cdot 4\text{H}_2\text{O}$ ,  $\geq 99.9\%$ ), potassium hydroxide standard solution (1 M, 99%), ethanol ( $\text{C}_2\text{H}_5\text{OH}$ , 99.7%) and polyvinylpyrrolidone (PVP) were obtained from Aladdin Reagent. Nafion (5 wt % solution in aliphatic alcohols and water) and ruthenium oxide ( $\text{RuO}_2$ ,  $\geq 99.9\%$ ) were purchased from Sigma-Aldrich. Commercial 20 wt% Pt/C was purchased from Johnson Matthey. All chemicals were used as received without any further purification. Deionized water ( $18.0 \text{ M}\Omega \cdot \text{cm}$ ) was used for preparing electrolyte solutions in all experiments.

### **Synthesis of NiFe@N-CFs**

The disposable bamboo sticks were collected and employed as starting materials. Typically, cleaned bamboo sticks were firstly whittled into bamboo shavings using penknife and then 1 g dry bamboo shavings were immersed into 70 mL of KOH aqueous solution ( $3 \text{ mol} \cdot \text{L}^{-1}$ ). After 30-min ultrasonication treatment, the resulting sample was transferred into a 100 mL Teflon-lined autoclave, which was sealed and placed in an electric oven at  $150 \text{ }^\circ\text{C}$  for 12 h. After being cooled down to room temperature naturally, the cotton-like products were collected by vacuum filtration, washed with deionized water for several times and dried in vacuum oven at  $60 \text{ }^\circ\text{C}$ . Next, approximately 0.2 g of the cotton-like products was immersed into 50 mL of ethanol solution containing metal ions (the molar ratios of  $\text{Fe}^{2+} : \text{Ni}^{2+} = 1:1$ ) and polyvinylpyrrolidone (PVP,  $2 \text{ mg mL}^{-1}$ ) for 30 min and dried naturally. Finally, the

NiFe@N-CFs was obtained by a thermostatic carbonization process at 800 °C for 2 h with a ramp rate of 5 °C min<sup>-1</sup> under a flow of high purity argon gas. Other NiFe@N-CFs samples were also prepared by adjusting the concentration of added Fe<sup>2+</sup> and Ni<sup>2+</sup>.

As the control experiments, the N-CFs sample was synthesized by the similar method but in the absence of metal ions; the CFs sample was prepared following the similar procedure but without both PVP and metal ions.

### **Physical characterization**

The powder X-ray diffraction (XRD) patterns were recorded on an X-ray diffractometer (Bruker Focus D8) with Cu K $\alpha$  radiation ( $\lambda = 1.54178 \text{ \AA}$ , 40 kV and 40 mA). The scanning electron microscope (SEM) was conducted on a Hitachi S-4800 (Hitachi, Japan) to obtain the surface morphology and structure. The transmission electron microscopy (TEM) images, high resolution transmission electron microscopy (HRTEM) images, and energy-dispersive X-ray spectroscopy (EDS) elemental mapping images were collected on a microscope (JEM2100F, JEOL, Japan) with an accelerating voltage of 200 kV. The specific surface areas and mesoporous pore size distribution of samples were determined by Brunauer-Emmett-Teller (BET) and Barrett-Joyner-Halenda (BJH) method. The surface compositions and valence states of samples were obtained by X-ray photoelectron spectroscopy (XPS) measurements performed on an ESCALAB 250Xi system from Thermo Fisher equipped with a hemispherical energy analyzer and a monochromatic Al K $\alpha$  source and C 1s peak at 284.8 eV was utilized as the reference for calibration.

### **Electrochemical measurements**

The ORR and OER electrocatalytic activities of catalysts were evaluated using a CHI760E electrochemical workstation (Shanghai Chenhua, China) coupled with a Pine rotator in 0.1 M KOH electrolyte, in which graphite rod and Hg/HgO (1 M KOH) electrode were used as counter and reference electrode, respectively. For ORR measurements, a glassy carbon rotating disk electrode (RDE) or rotating ring disk electrode (RRDE) coated with catalyst ink was used as the working electrode. For OER measurements, the experiments were conducted in a stationary solution. Homogeneous catalysts inks were prepared by dispersing 4 mg of the catalysts and 80  $\mu$ L 5 wt% Nafion solution into 1 mL ethanol. After ultrasonication for 30 min, the catalyst slurry was evenly dropped onto the pre-polished working electrode. All potentials and current densities in this paper were normalized to the reversible hydrogen electrode (RHE) based on the Nernst equation ( $E_{\text{RHE}} = E_{\text{Hg/HgO}} + 0.059 \times \text{pH} + 0.098$ ) and the geometric area of the electrode.

For the OER, linear sweep voltammetry (LSV) profiles were obtained at a scan rate of 5  $\text{mV s}^{-1}$  in the potential range of 0.2 - 1 V (vs. Hg/HgO). Before the LSV test, continuous cyclic voltammetry (CV) scans were carried out at a scan rate of 10  $\text{mV s}^{-1}$  within the same potential range until stabilization. The Tafel slopes for evaluating the OER kinetics of the catalysts were calculated by plotting overpotential  $\eta$  against log current density ( $j$ ) from LSV curves. Electrochemical impedance spectroscopy (EIS) was collected at various overpotentials in the frequency range from 0.01 Hz to 100 KHz with an amplitude of 5 mV. The electrochemical active surface areas (ECSA) of catalysts are proportional to the double-layer capacitance ( $C_{\text{dl}}$ ). The  $C_{\text{dl}}$  was estimated

by measuring CV in a non-faradaic region (1.0 - 1.1 V) at different scan rates (40, 60, 80, 100 and 120 mV s<sup>-1</sup>). The capacitive currents  $\Delta J$  ( $J_a - J_c$ ) at 1.05 V against scan rate were fitted to acquire the  $C_{dl}$  using  $C_{dl} = \Delta J/2\nu$  ( $\nu$  is the scan rate). The chronoamperometric measurement with a current density of 10 mA cm<sup>-2</sup> was applied to evaluate the stability of electrocatalysts. All the data were presented without iR correction.

The RDE polarization curves for ORR were performed in O<sub>2</sub>-saturated 0.1 M KOH at different rotation speeds from 400 to 2025 rpm with a sweep rate of 5 mV s<sup>-1</sup>. The kinetic current ( $J_k$ ) and electron transfer number ( $n$ ) were calculated using the Koutecky-Levich equation:

$$\frac{1}{J} = \frac{1}{J_L} + \frac{1}{J_K} = \frac{1}{B\omega^{1/2}} + \frac{1}{J_K}$$

$$B = 0.62nFC_0(D_0)^{2/3}\nu^{-1/6}$$

where  $J$ ,  $J_L$  and  $J_k$  are the measured, diffusion limiting and kinetic current density, respectively;  $F$  is the Faraday constant (96485 C mol<sup>-1</sup>);  $C_0$  is the bulk concentration of O<sub>2</sub> (1.2×10<sup>-3</sup> mol L<sup>-1</sup>);  $D_0$  is the diffusion coefficient of O<sub>2</sub> (1.9×10<sup>-5</sup> cm<sup>2</sup> s<sup>-1</sup>);  $\nu$  is the kinetic viscosity of electrolyte (0.01 cm<sup>2</sup> s<sup>-1</sup>) and  $\omega$  is the angular velocity of disk ( $\omega = 2\pi r$ ,  $r$  is the linear rotation speed).

RRDE measurements were also applied to determine the electron transfer number ( $n$ ) and the yield of hydrogen peroxide (H<sub>2</sub>O<sub>2</sub>%) released during ORR, which were calculated based on the following equations:

$$n = 4 \times \frac{I_d}{I_r/N + I_d}$$

$$\text{H}_2\text{O}_2 (\%) = 200 \times \frac{I_r/N}{I_r/N + I_d}$$

where  $I_d$  is the disk current,  $I_r$  is the ring current and  $N$  is the current collection efficiency (0.37) of the Pt ring of RRDE electrode. The ring potential was set to a constant value of 0.35 V vs. Hg/HgO.

### **Assembly of rechargeable Zinc-air battery**

The home-made liquid rechargeable Zn-air batteries were fabricated, where hydrophobic carbon paper with as-prepared catalysts (loading amount of 1.5 mg cm<sup>-2</sup>) as the air cathode and polished Zn plate (0.2 mm of thickness) as the anode, respectively, and 6 M KOH containing 0.2 M zinc acetate solution was used as the electrolyte to ensure reversible Zn electrochemical reaction. For comparison, a mixture of Pt/C and RuO<sub>2</sub> catalyst with a mass ratio of 1:1 was also used as reference bifunctional air electrodes. The polarized profiles were recorded using LSV at the scan rate of 5 mV s<sup>-1</sup>. Galvanostatic discharge-charge cycling tests were carried out to evaluate the catalyst durability; in each Galvanostatic cycle, the discharge and charge period was set to be 20 min at a given current density of 10 mA cm<sup>-2</sup>. The specific capacity was calculated according the following equation:

$$\text{Specific capacity} = \frac{\text{current} * \text{service hours}}{\text{weight of consumed zinc}}$$

### **Fabrication of the Quasi-solid-state Zn-Air Batteries**

The NiFe@N-CFs was directly used as the flexible, self-supporting air cathode, and a polished flexible zinc foil (0.1 mm thickness) served as the anode. The PVA gel polymer electrolyte was prepared as follows: 1.0 g polyvinyl alcohol (PVA) powder (MW ~19500, Aladdin) was dissolved in 10 mL deionized water at 95 °C under magnetic stirring for about 2 h. Next, 1 mL of 18 M KOH aqueous solution containing 0.2 M zinc acetate was added into the former solution and continuously stirred until the solution became clear. After that, the solution was poured onto a glass plate to form a thin electrolyte film. The film was kept in a freezer at -4 °C over 12 h, and then thawed at room temperature. The quasi-solid-state Zn-air battery was assembled by placing NiFe@N-CFs and zinc foil on the two sides of PVA gel film wetted by 6 M KOH electrolyte and a piece of pressed Ni foam was used as current collector outside the air cathode.

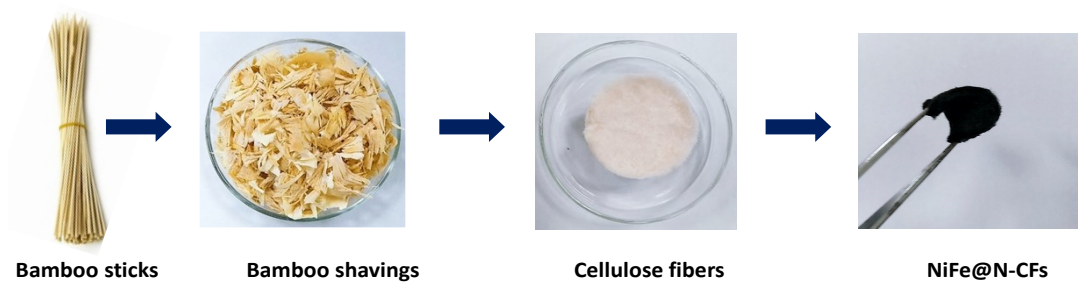


**Figure S1.** Optical images of the materials obtained in each step during the synthesis of NiFe@N-CFs.

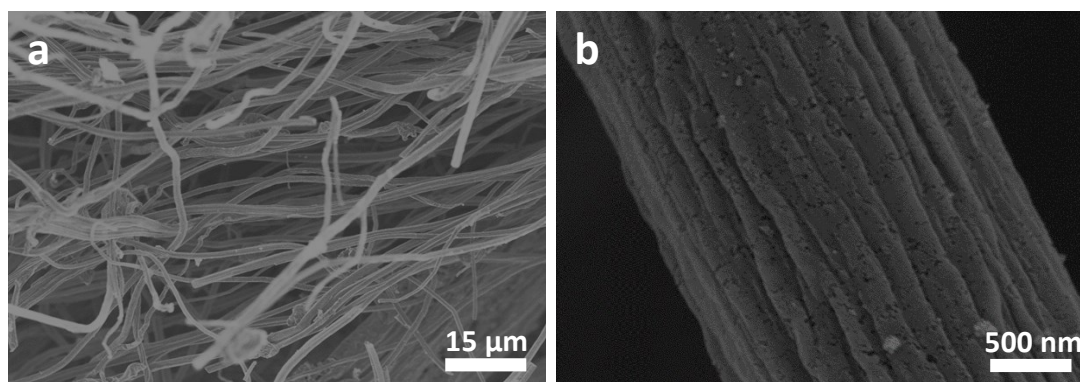


**Figure S2.** SEM images of cellulose fibers at (a) low and (b) high magnifications.

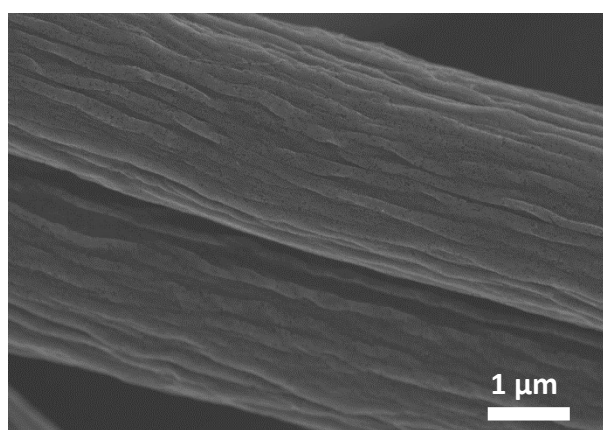


**Figure S3.** SEM image of N-CFs synthesized without NiFe loading.

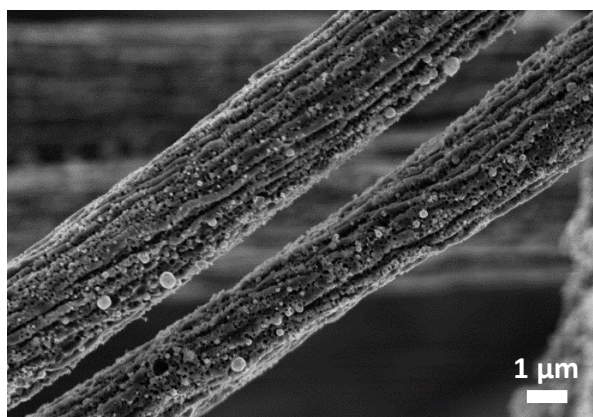


**Figure S4.** SEM image of NiFe@N-CFs synthesized without PVP.

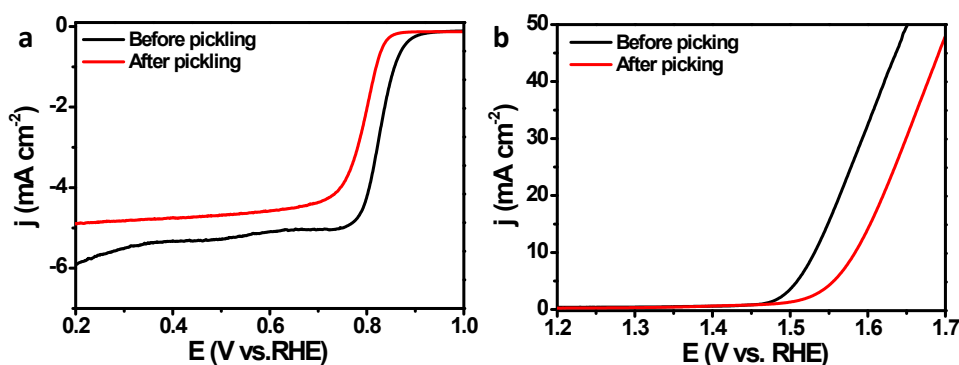


**Figure S5.** (a) ORR and (b) OER polarization curves of NiFe@N-CFs before and after acid washing.

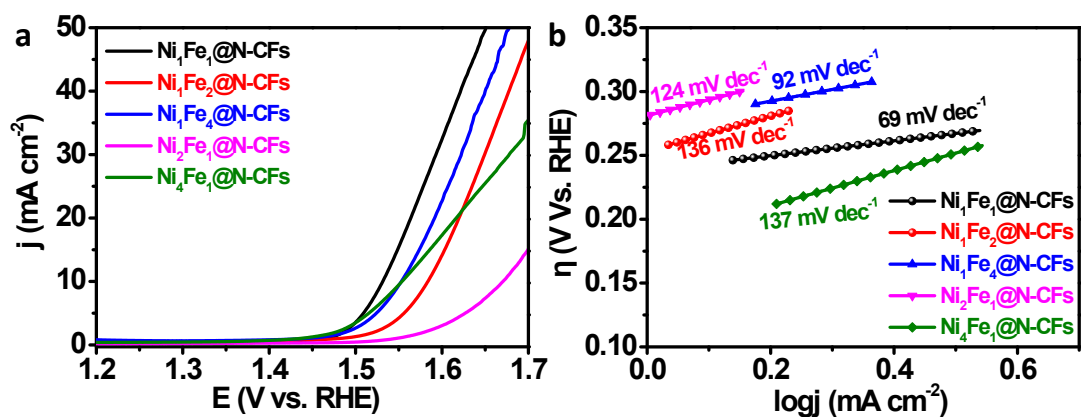


**Figure S6.** (a) The OER polarization curves and (b) corresponding Tafel plots of the catalysts with different Ni/Fe ratios.

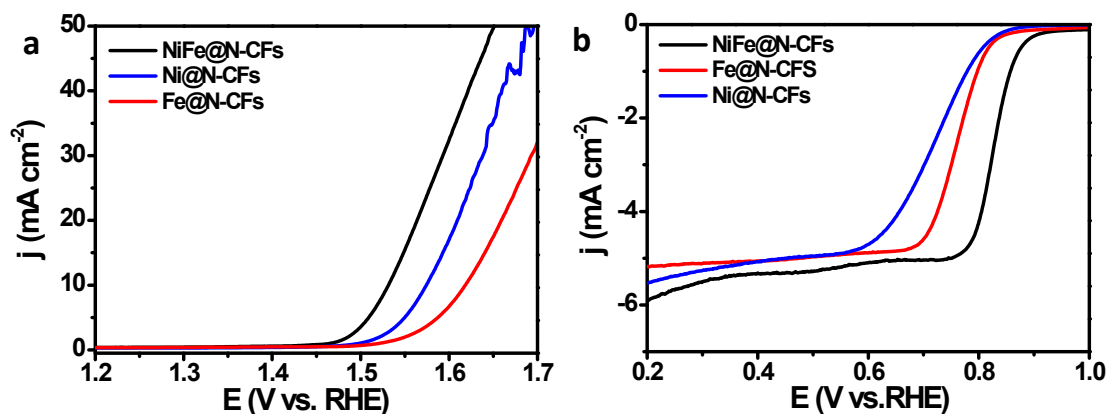


**Figure S7.** (a) OER and (b) ORR polarization curves of Ni@N-CFs, Fe@N-CFs and NiFe@N-CFs.

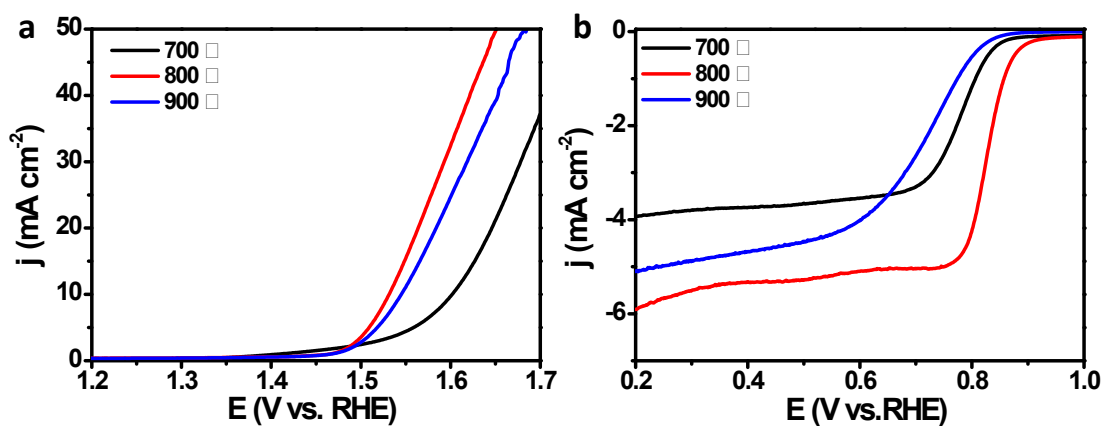


**Figure S8.** (a) OER and (b) ORR polarization curves of NiFe@N-CFs obtained at different temperatures of 700, 800, and 900 °C, respectively. As can be seen, NiFe@N-CFs obtained at 800 °C exhibits the best activity.

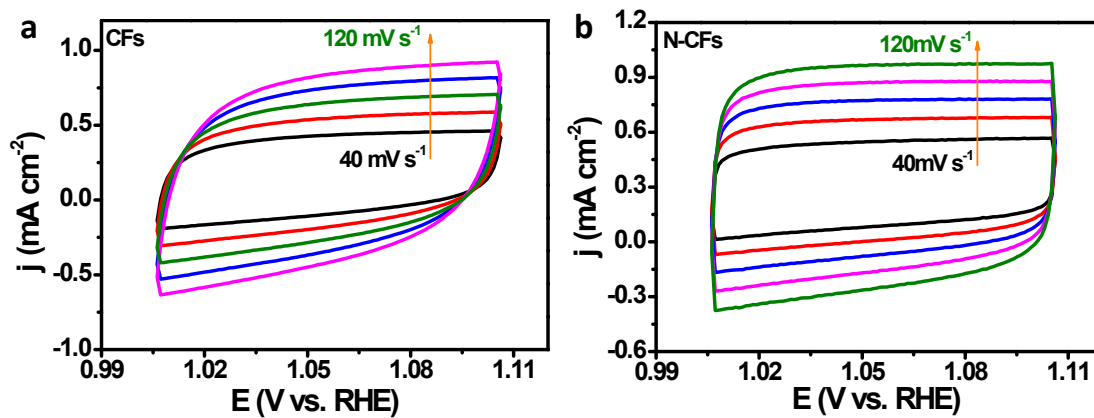


**Figure S9.** CVs of (a) CFs and (b) N-CFs at different scan rates.

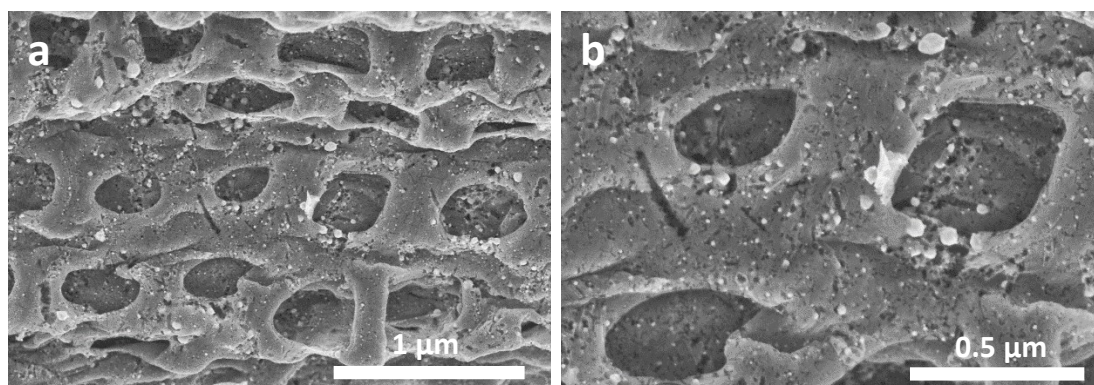
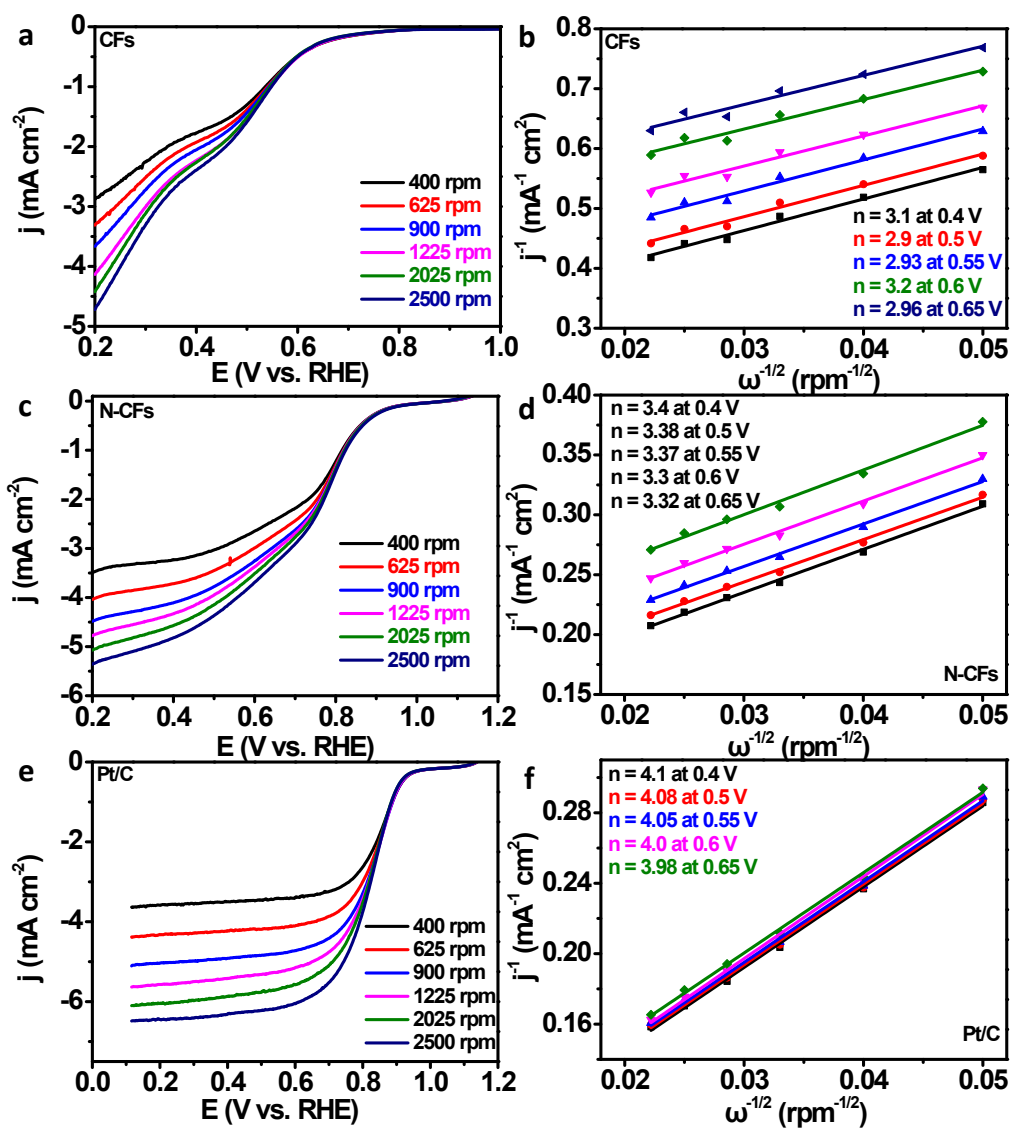


**Figure S10.** SEM images of NiFe@N-CFs after OER test: (a) low magnification, (b) high magnification.



Figure

e S11. (a, c, e) LSV curves of as-prepared catalysts at different rotating speeds and (b, d, f) K-L plots at different potentials including the calculated electron transfer number ( $n$ ).

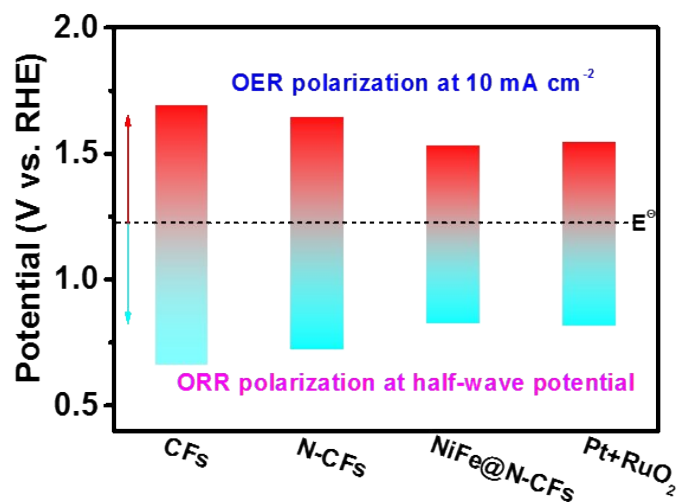


**Figure S12.** Potential difference between ORR  $E_{1/2}$  and OER  $E_{j=10}$  of various electrocatalysts.

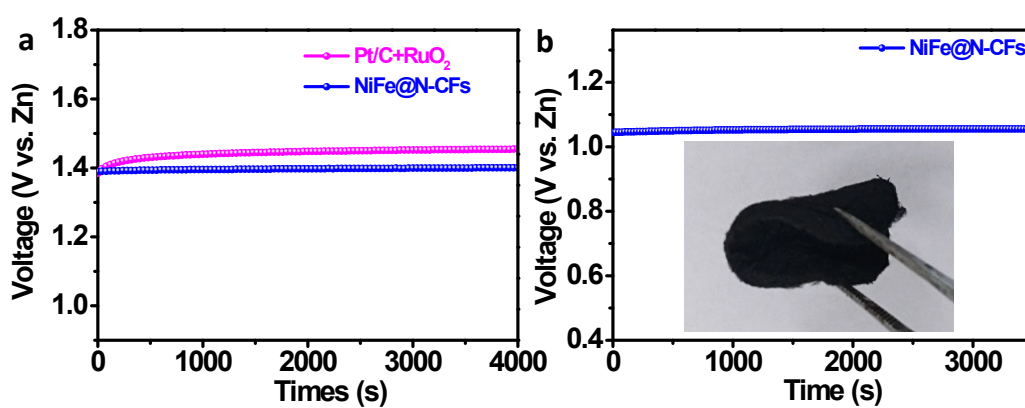


**Figure S13.** Curves of open-circuit potential versus time for the battery based on NiFe@N-CFs: (a) liquid Zn-air battery, (b) quasi-solid-state Zn-air battery (inset: photograph of the free-standing NiFe@N-CFs electrode).

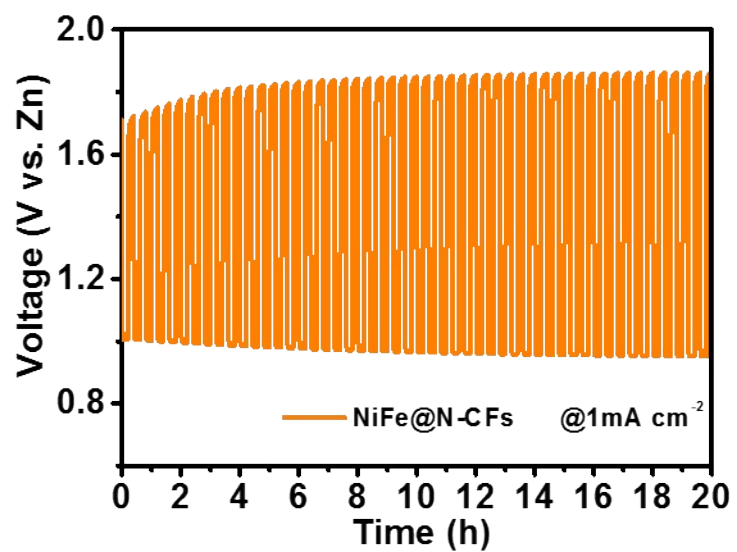


**Figure S14.** Cycling performance of the flexible quasi-solid-state Zn-air battery with NiFe@N-CFs cathode at a current density of  $1 \text{ mA cm}^{-2}$ .

**Table S1.** Comparison of the ORR/OER activities of NiFe@N-CFs catalyst with recently reported bifunctional electrocatalysts.

Catalysts	ORR:	OER:	$\Delta E=$	Reference
	$E_{1/2}$ (V)	$E_{j=10}$ (V)	$E_{j=10}-E_{1/2}$ (V)	
NiFe@N-CFs	0.82	1.53	0.71	This work
NiFe/N-CNT	0.75	1.52	0.77	1
FeNi-NC	0.83	1.61	0.78	2
Fe <sub>1</sub> Co <sub>1</sub> -NC <sub>ps</sub>	0.84	1.61	0.76	3
NiCo/PFC	0.79	1.63	0.84	4
N-GCNT/FeCo	0.92	1.73	0.81	5
Ni <sub>3</sub> FeN	0.78	1.58	0.80	6
Ni <sub>3</sub> Fe/N-C sheets	0.76	1.60	0.84	7
CoFe/N-GCT	0.79	1.67	0.88	8
NiCo@N-C2	0.81	1.76	0.95	9
Ni <sub>3</sub> FeN/NRGO	0.72	1.63	0.91	10
Co-N <sub>x</sub> - graphene	1.73	0.78	0.95	11
Co <sub>3</sub> O <sub>4</sub> /PGC	0.68	1.77	1.09	12

**Table S2.** The performance of liquid rechargeable Zn-air batteries with various bifunctional oxygen electrocatalysts reported in literature.

Catalyst	Peak power density (mW cm <sup>-2</sup> )	charge/discharge voltage gap (V)	Specific capacity (mAh g <sub>Zn</sub> <sup>-1</sup> )	Stability	Reference
NiFe@N-CFs	102	0.66@10 mA cm <sup>-2</sup>	719@5 mA cm <sup>-2</sup>	20 min/cycle @10 mA cm <sup>-2</sup> for 300 Cycles, no significant voltage gap change	This work
CoS <sub>2</sub> /SKJ	104	0.92@25 mA cm <sup>-2</sup>	N/A	40 min/cycle@25 mA cm <sup>-2</sup> for 255 cycles, no significant voltage gap change	13
CoNi@NCN T/NF	127	0.84@10 mA cm <sup>-2</sup>	655@5 mA cm <sup>-2</sup>	30 min/cycle@5 mA cm <sup>-2</sup> for 90 cycles, voltage gap increased ~0.27 V	14
FeNi-NC	80.8	0.82@8 mA cm <sup>-2</sup>	N/A	10 min/cycle@8 mA cm <sup>-2</sup> for 69 cycles, no significant voltage gap change	2
Co/N-CNSNs	81.7	0.79@10 mA cm <sup>-2</sup>	638@10 mA cm <sup>-2</sup>	20 min/cycle @10 mA cm <sup>-2</sup> for 100 cycles, voltage gap increased ~0.15 V	15
NiO/CoN PINWs	79.6	0.84@20 mA cm <sup>-2</sup>	690@5 mA cm <sup>-2</sup>	10 min/cycle@charge current of 50 mA cm <sup>-2</sup> and discharge current of 1 mA cm <sup>-2</sup> for 50 cycles	16
Co-N, B-CSs	100.4	1.35@20 mA cm <sup>-2</sup>	N/A	5 min/cycle@5 mA cm <sup>-2</sup> for 128 cycles, voltage gap increased ~0.2 V	17
Fe@C-NG/NCNTs	101.2	0.89@10 mA cm <sup>-2</sup>	682@10 mA cm <sup>-2</sup>	20 min/cycle@10 mA cm <sup>-2</sup> for 297 cycles, voltage gap increased ~0.12 V	18
CoNi/BCF	155	N/A	711@10 mA cm <sup>-2</sup>	10 min/cycle@10 mA cm <sup>-2</sup> for 90 cycles, no significant voltage gap change	19
CoN <sub>4</sub> /NG	115	0.84@10 mA cm <sup>-2</sup>	730@10 mA cm <sup>-2</sup>	40 min/cycle@10 mA cm <sup>-2</sup> for 150 cycles, no significant voltage gap change	20
FeNiCo@NC-P	112	0.84@10 mA cm <sup>-2</sup>	N/A	30min/cycle@10 mA cm <sup>-2</sup> for 90 cycles, voltage gap increased ~0.3 V	21

## Supplementary references

- 1 H. Lei, Z. Wang, F. Yang, X. Huang, J. Liu, Y. Liang, J. Xie, M. S. Javed, X. Lu, S. Tan and W. Mai, *Nano Energy*, 2019, **68**, 104293.
- 2 L. Yang, X. Zeng, D. Wang and D. Cao, *Energy Storage Mater*, 2018, **12**, 277-283.
- 3 J. Liu, T. He, Q. Wang, Z. Zhou, Y. Zhang, H. Wu, Q. Li, J. Zheng, Z. Sun and Y. Lei, *J. Mater. Chem. A*, 2019, **7**, 12451-12456.
- 4 G. Fu, Y. Chen, Z. Cui, Y. Li, W. Zhou, S. Xing, Y. Tang and J. B. Goodenough, *Nano Lett.*, 2016, **16**, 6516-6522.
- 5 S. H. Ahn and A. Manthiram, *Small*, 2017, **13**, 1702068.
- 6 H. B. Yang, J. Miao, S.-F. Hung, J. Chen, H. B. Tao, X. Wang, L. Zhang, R. Chen, J. Gao, H. M. Chen, L. Dai and B. Liu, *Sci. Adv.* 2016, **2**, 1501122.
- 7 G. Fu, Z. Cui, Y. Chen, Y. Li, Y. Tang and J. B. Goodenough, *Adv. Energy Mater.*, 2017, **7**, 1601172.
- 8 X. Liu, L. Wang, P. Yu, C. Tian, F. Sun, J. Ma, W. Li and H. Fu, *Angew. Chem. Int. Ed.*, 2018, **57**, 16166-16170.
- 9 Y. Fu, H.-Y. Yu, C. Jiang, T.-H. Zhang, R. Zhan, X. Li, J.-F. Li, J.-H. Tian and R. Yang, *Adv. Funct. Mater.*, 2018, **28**, 1705094.
- 10 Y. Fan, S. Ida, A. Staykov, T. Akbay, H. Hagiwara, J. Matsuda, K. Kaneko and T. Ishihara, *Small*, 2017, **13**, 1700099.
- 11 S. Chen, L. Ma, S. Wu, S. Wang, Z. Li, A. A. Emmanuel, M. R. Huqe, C. Zhi and J. A. Zapien, *Adv. Funct. Mater.*, 2020, **30**, 1908945.
- 12 J. N. Liu, B. Q. Li, C. X. Zhao, J. Yu and Q. Zhang, *ChemSusChem*, 2019, **13**, 1-9.

- 13 Z. Zhang, Y.-P. Deng, Z. Xing, D. Luo, S. Sy, Z. P. Cano, G. Liu, Y. Jiang and Z. Chen, *Acs Nano*, 2019, **13**, 7062-7072.
- 14 W. Niu, S. Pakhira, K. Marcus, Z. Li, J. L. Mendoza-Cortes and Y. Yang, *Adv. Energy Mater.*, 2018, **8**, 1800480.
- 15 X. Huang, Y. Zhang, H. Shen, W. Li, T. Shen, Z. Ali, T. Tang, S. Guo, Q. Sun and Y. Hou, *ACS Energy Lett.*, 2018, **3**, 2914-2920.
- 16 J. Yin, Y. Li, F. Lv, Q. Fan, Y. Q. Zhao, Q. Zhang, W. Wang, F. Cheng, P. Xi and S. Guo, *ACS Nano*, 2017, **11**, 2275-2283.
- 17 Y. Guo, P. Yuan, J. Zhang, Y. Hu, I. S. Amiin, X. Wang, J. Zhou, H. Xia, Z. Song, Q. Xu and S. Mu, *ACS Nano*, 2018, **12**, 1894-1901.
- 18 Q. Wang, Y. Lei, Z. Chen, N. Wu, Y. Wang, B. Wang and Y. Wang, *J. Mater. Chem. A*, 2018, **6**, 516-526.
- 19 W. Wan, X. Liu, H. Li, X. Peng, D. Xi and J. Luo, *Appl. Catal. B-Environ.*, 2019, **240**, 193-200.
- 20 L. Yang, L. Shi, D. Wang, Y. Lv and D. Cao, *Nano Energy*, 2018, **50**, 691-698.
- 21 D. Ren, J. Ying, M. Xiao, Y. P. Deng, J. Ou, J. Zhu, G. Liu, Y. Pei, S. Li, A. M. Jauhar, H. Jin, S. Wang, D. Su, A. Yu and Z. Chen, *Adv. Funct. Mater.*, 2019, **30**, 1908167.